Reticular Pseudodrusen Are Associated With More Advanced Para-Central Photoreceptor Degeneration in Intermediate Age-Related Macular Degeneration

Matt Trinh,[1,2] Natalie Eshow,[1,2] David Alonso-Caneiro,[3] Michael Kalloniatis,[1,2,4] and Lisa Nivison-Smith[1,2]

[1]Centre for Eye Health, University of New South Wales, Sydney, New South Wales, Australia
[2]School of Optometry and Vision Science, University of New South Wales, Sydney, New South Wales, Australia
[3]Contact Lens and Visual Optics Laboratory, Queensland University of Technology, Brisbane, Queensland, Australia
[4]School of Medicine (Optometry), Deakin University, Geelong, Victoria, Australia

Correspondence: Lisa Nivison-Smith, School of Optometry and Vision Science, University of New South Wales (UNSW) Sydney, 2052, New South Wales, Australia; l.nivison-smith@unsw.edu.au.

Received: June 29, 2022
Accepted: September 19, 2022
Published: October 17, 2022

Citation: Trinh M, Eshow N, Alonso-Caneiro D, Kalloniatis M, Nivison-Smith L. Reticular pseudodrusen are associated with more advanced para-central photoreceptor degeneration in intermediate age-related macular degeneration. *Invest Ophthalmol Vis Sci.* 2022;63(11):12. https://doi.org/10.1167/iovs.63.11.12

Purpose. The purpose of this study was to examine retinal topographical differences between intermediate age-related macular degeneration (iAMD) with reticular pseudodrusen (RPD) versus iAMD without RPD, using high-density optical coherence tomography (OCT) cluster analysis.

Methods. Single eyes from 153 individuals (51 with $iAMD_{+RPD}$, 51 with iAMD, and 51 healthy) were propensity-score matched by age, sex, and refraction. High-density OCT grid-wise (60 × 60 grids, each approximately 0.01 mm^2 area) thicknesses were custom-extracted from macular cube scans, then compared between $iAMD_{+RPD}$ and iAMD eyes with correction for confounding factors. These "differences (µm)" were clustered and results de-convoluted to reveal mean difference (95% confidence interval [CI]) and topography of the inner retina (retinal nerve fiber, ganglion cell, inner plexiform, and inner nuclear layers) and outer retina (outer plexiform/Henle's fiber/outer nuclear layers, inner and outer segments, and retinal pigment epithelium-to-Bruch's membrane [RPE-BM]). Differences were also converted to Z-scores using normal data.

Results. In $iAMD_{+RPD}$ compared to iAMD eyes, the inner retina was thicker (up to +5.89 [95% CI = +2.44 to +9.35] µm, $P < 0.0001$ to 0.05), the outer para-central retina was thinner (up to −3.21 [95% CI = −5.39 to −1.03] µm, $P < 0.01$ to 0.001), and the RPE-BM was thicker (+3.38 [95% CI = +1.05 to +5.71] µm, $P < 0.05$). The majority of effect sizes (Z-scores) were large (−3.13 to +1.91).

Conclusions. OCT retinal topography differed across all retinal layers between iAMD eyes with versus without RPD. Greater para-central photoreceptor thinning in RPD eyes was suggestive of more advanced degeneration, whereas the significance of inner retinal thickening was unclear. In the future, quantitative evaluation of photoreceptor thicknesses may help clinicians monitor the potential deleterious effects of RPD on retinal integrity.

Keywords: reticular pseudodrusen (RPD), subretinal drusenoid deposits, age-related macular degeneration (AMD), anatomy, clustering, optical coherence tomography (OCT), spatial, retinal thickness

Reticular pseudodrusen (RPD; also known as sub-retinal drusenoid deposits)[1] are sub-retinal granular extracellular deposits containing photoreceptor and retinal pigment epithilium (RPE) byproducts.[2–5] RPD in the presence of age-related macular degeneration (AMD) are important to recognize as they may be associated with greater risk of progression to late AMD,[6–10] although some studies have suggested otherwise.[11–14] AMD with RPD has also been associated with faster progression of geographic atrophy,[15] poorer response to AMD treatments,[16,17] and worse visual sensitivity when compared to AMD without RPD.[18]

To better understand why the RPD phenotype may (or may not) confer worse outcomes in patients with AMD, several studies have investigated the effects of RPD on in vivo retinal anatomy and yielded conflicting results. For example, eyes with early and/or intermediate AMD (iAMD) with RPD have been found to have total retinal thickness both thinned[19,20] or non-different[19–23] compared to early/iAMD eyes without RPD. Similarly, inner retinal thickness has been reported to be thickened[24,25] or non-different,[25,26] and outer retinal thickness has been reported to be thinned,[24–29] thickened,[23,24] or non-different[23,25–28] in early/iAMD eyes with RPD versus without RPD.

Dissimilarities in study characteristics, such as varying population demographics and methods of RPD identification/grading,[18] may explain some of the discrepancies

in the aforementioned studies. However, more notably, all these studies make the a priori assumption that retinal changes will follow an existing spatial template, such as predefined points,[20,22,28] the Early Treatment Diabetic Retinopathy Study (ETDRS) sectors,[19,21,23,25,27,29] or large/global areas.[24,26] These arbitrary spatial groupings introduce statistical bias known as the modifiable areal unit problem (MAUP),[30,31] whereby results may be misrepresented or even masked depending upon how data are spatially grouped (e.g. via the aforementioned spatial templates).

Recently, we addressed the MAUP by sampling the macula using 3600 or 60 × 60 OCT grids across each individual retinal layer. These grids could not be further meaningfully divided, resulting in data sets of nonmodifiable high-density grid-wise retinal layer thicknesses.[32–35] To avoid any a priori spatial grouping of data which would induce the MAUP, we then applied unsupervised cluster analysis post hoc to classify grids into clusters that were statistically similar within-cluster and statistically separable between clusters. This method revealed in vivo retinal anatomical topographies of AMD and normal aging eyes[32–36] that have otherwise been undetectable via arbitrary spatial groupings, such as the ETDRS sectors. For example, using this method, we found extensive spatial patterns of thinning with large effect sizes across each individual retinal layer, suggesting that retinal-spanning degenerative changes begin at the early stage of AMD.[35]

Thus, in this study, we aimed to use high-density optical coherence tomography (OCT) cluster analysis to resolve the MAUP and clarify the potential effects of RPD on retinal topography in iAMD. We hypothesize that RPD presence is associated with greater thinning in iAMD eyes, particularly at the photoreceptor layers. These results could help answer whether RPD is associated with more advanced degeneration in iAMD and improve understanding of where in the retina RPD may impact, thus guiding clinical monitoring and future intervention protocol.

Methods

Study Population

The study population was recruited through retrospective review of all patient records from the Centre for Eye Health (CFEH) Sydney, Australia, from January 1, 2009, to December 31, 2021. CFEH is a referral-based clinic with advanced diagnostic testing and management of eye disease by optometrists and ophthalmologists.[37] All patients who had their records reviewed had provided prior written informed consent for research use of their de-identified data approved by the Biomedical Human Research Ethics Advisory Panel of the University of New South Wales and in accordance with the Declaration of Helsinki.

All participants regardless of study group were required to be ≥50 years of age and have no macular-involving disease or significant structural abnormality (except RPD and/or iAMD for the respective study groups). Optic neuropathies (including suspected or confirmed glaucoma) were excluded due to partial macular involvement. All diagnoses were formed by two non-blind CFEH clinicians (optometrists and/or ophthalmologists) and confirmed by investigator author Matt Trinh. A single eye was selected for each participant, and simple randomization was used if both eyes were eligible. Systemic factors, including self-reported presence of diabetes mellitus (type 1 or 2),[38] smoking (ever or never),[39,40] and hypertension,[40] which have some (conflicting)[41–46] evidence of association with retinal thicknesses, were compared between groups after propensity-score matching. These factors were not included in propensity-score matching to preserve sample size, considering increased prevalence of these systemic factors with age.[47,48]

Eligibility of iAMD$_{+RPD}$ eyes required the presence of RPD based on the study by Ueda-Arakawa et al.[49] (i.e. ≥5 hyperreflective lesions above the RPE via OCT, and iAMD based on a modified Beckman Initiative classification[50]; i.e. presence of large drusen [≥125 µm] or pigmentary abnormalities related to AMD with at least medium drusen via color fundus photography).[50] Other imaging modalities, such as color fundus photography, near-infrared, and fundus autofluorescence, were available for all patients screened for eligibility as part of standard CFEH clinical care and used to aid diagnoses and exclude other ocular pathology. Participants aged 50 to 54 years were included if iAMD phenotypic criteria were fulfilled in concordance with other notable studies.[12,51–53] Eligibility of iAMD eyes required the presence of iAMD without RPD. Eligibility of normal healthy eyes required visual acuity better than 0.1 logMAR for participants <60 years or 0.2 logMAR for participants ≥60 years, the latter criteria being more lenient to account for normal age-related decline of visual acuity from numerous factors, including cataracts.[54–57]

Propensity-Score Matching

The iAMD$_{+RPD}$ eyes were propensity-score matched to iAMD eyes and then normal eyes using multi-variable logistic regression considering age, sex, and spherical equivalent refraction as co-variables. Fuzzy matching without replacement was performed to randomize selection of participants, whereas mitigating imbalance of potential confounders between groups, as opposed to exact matching which can significantly reduce sample size in a limited sampling pool and increase selection bias.[58,59] Match tolerance of propensity scores was increased after iterative random draws until maximal sample size.[60]

Image Acquisition and Retinal Layer Segmentation

OCT macular cube scans across an area of 30 × 25 degrees or approximately 8640 × 7200 µm (width × height) were acquired from the Spectralis SD-OCT (Heidelberg Engineering, Heidelberg, Germany). The width was parallel to the axis between the fovea-to-optic nerve head center and the height perpendicular to this width. All conversions between retinal µm and degrees were performed under the model approximation that 1 degree = approximately 288 µm[61–63] which maintains a relatively linear relationship within the retinal (non-peripheral) area analyzed in this study.[61] The scanning protocol contained 61 B-scans spaced approximately 118 µm apart, which was the highest number of B-scans commercially available for the Spectralis SD-OCT without significant compromise in image quality.[62] If multiple scans per participant were eligible for inclusion, the latest scan above 15 dB signal strength and without significant artifacts was selected. Ocular tilt, automatic segmentation, and then manual correction of segmentation were applied

to each scan via the HRA/Spectralis Viewing Module 6.9.5.0 (Heidelberg Engineering).

As previously described,[32–35] each participant was randomized into one of two blocks, and each block had their selected OCT macular cube scans independently reviewed by two observers (authors M.T. and N.E.). Retinal layer segmentation for the retinal nerve fiber layer (RNFL), ganglion cell layer (GCL), inner plexiform layer (IPL), inner nuclear layer (INL), outer plexiform layer (OPL)/Henle's fiber layer (HFL)/outer nuclear layer (ONL), IS/OS, and RPE-Bruch's membrane (BM) were manually corrected where necessary (Fig. 1A, pink insert). Due to inconsistent reflectivity with Henle's fibers in the OPL/HFL/ONL[35,64] and disrupted photoreceptor ellipsoid in the IS/OS,[65] particularly in diseased eyes, these layers were combined from their respective individual layers. The alternate block was then reviewed by authors Matt Trinh and Natalie Eshow, and further manual correction performed after discussion and consensus. There was non-blinding to study group as drusen and/or pigmentary changes are obvious during the segmentation process. Manual correction of segmentation was used as the "ground-truth" for retinal anatomy in concordance with other studies,[66–68] and has demonstrated excellent repeatability and reproducibility for AMD eyes.[69]

Segmentations were manually corrected to continue through (rather than around) large vessels to mitigate effect on thicknesses (see Fig. 1A, asterisk). Segmentations were also manually corrected around conventional drusen and RPD (see Fig. 1A, black arrowhead). Regarding RPD, the middle of the external limiting membrane was segmented to continue through RPD apices (for RPD significantly protruding toward the inner retina)[70] and the RPE was segmented to continue under RPD (see Fig. 1A, white arrowheads), in correspondence with histology.[4]

High-density OCT Thickness Comparison Between iAMD$_{+RPD}$ and iAMD Eyes

Custom-extraction of thicknesses was executed using MATLAB (version 9.9; MathWorks, Natick, MA, USA) code developed by investigator author David Alonso-Caneiro and applied to OCT macular volume RAW and XML files with adjustment for foveal location and foveal-to-optic nerve head tilt.[71] This code enabled sampling and averaging of the volumetric OCT dataset into 3600 grids (60 × 60 grids, each approximately 0.01 mm^2 area, comprised of or 0.4 × 0.4 degrees or approximately 115 × 115 µm sides; i.e. thicknesses, foveally centered and covering 24 × 24 degrees or approximately 6912 × 6912 µm; Fig. 1B) across each retinal layer. Grid density of 60 × 60 was utilized to maximize coverage of the 61 B-scans per macular cube scan. Grid coverage of approximately 6912 × 6912 µm was in accordance with the default commercially available Spectralis Viewing Module grid coverage for 64 grids (8 × 8 grids, each approximately 0.75 mm^2 area). Note that grid coverage (24 × 24 degrees or approximately 6912 × 6912 µm) did not extend to the entire scan area (30 × 25 degrees or approximately 8640 × 7200 µm), but did include the entire macula (approximately 19 degrees diameter or approximately 5500 µm).[72]

Grid-wise thicknesses of iAMD$_{+RPD}$, iAMD, and normal groups across each retinal layer were used to develop multivariable linear regression models enabling correction for potential confounding from age, sex, refraction, presence of pigmentary abnormalities, and average RPE-BM thickness. Refraction was used as a proxy for axial length based on strong correlation between the two variables.[73] As a constituent of magnification correction factor,[74,75] the correction (and matching) of refraction also ensured that between-group analyses maintained statistical robustness regardless of within-group differences in magnification factors. Average RPE-BM thickness was included to account for differing drusen load between groups (except when comparing the RPE-BM between groups).

Grid$_{n/3600}$ of an iAMD$_{+RPD}$ eye would be subtracted by grid$_{n/3600}$ of an iAMD eye corrected to the same age, sex, refraction, presence of pigmentary abnormalities, and average RPE-BM thickness, resulting in grid$_{n/3600}$ difference (µm; see Fig. 1B). This process was repeated for all 3600 grids, for each retinal layer, and for all participants to account for potential confounding at the grid-wise level (pre-clustering) rather than the group level (post-clustering). This ensured that regression characteristics were not indiscriminately applied to all grids within each spatial group (cluster) which could otherwise introduce statistical bias known as the MAUP[30,31] (i.e. the potential misrepresentation of results dependent upon how data are spatially grouped and analyzed).

Clustering and Retinal Topography Between iAMD$_{+RPD}$ and iAMD Eyes

Grid-wise differences (µm) between iAMD$_{+RPD}$ and iAMD eyes were assigned into clusters which represented groupings of statistically similar values within clusters and statistically separable values between clusters.[76] Unsupervised cluster analysis was performed using the two-step algorithm due to its robustness compared to several other cluster algorithms.[77] Grid order was randomized[78] and a log-likelihood method[79] applied with consideration of the lowest Bayesian Information Criterion, intra-cluster similarity, and inter-cluster separability[80] to generate clusters for each individual retinal layer. The clustering process was reiterated until all clusters were separable by >95th percentile mean difference limits, ensuring that all clusters were significantly different ($P < 0.05$) from each other (Fig. 1C). Note that cluster confidence intervals (CIs) can overlap and still be significantly different, as separability by >95th percentile mean difference limits is approximately equal to separability of 84th percentile limits around individual means.[81,82]

Clusters were then de-convoluted to generate means (95% CI) displayed graphically (Fig. 1D, left) and patterns displayed topographically (see Fig. 1D, right). Clusters were labeled positive or negative then ranked based on magnitude of difference (µm; see Fig. 1D, middle legend). Differences were also converted to Z-scores (i.e. SD units from normal [corrected]), to demonstrate effect sizes. Non-zero cluster proportional areas (%) were reported to justify use of and compare descriptive spatial delineations for quadrants and centrality. Quadrants were defined as: superior, nasal, inferior, and temporal. Centrality was defined (anatomically)[72] as: "central macula" (approximately 5.2 degrees or approximately 1500 µm diameter), "peri-central macula" (approximately 7 degrees or approximately 2000 µm diameter ring), "para-central macula" (approximately 12.2 degrees or approximately 3500 µm diameter ring), "peripheral macula" (approximately 19 degrees or approximately 5500 µm diameter ring), and "extra-macula" (outside approximately 19 degrees or approximately 5500 µm diameter; see Fig. 1D,

Investigative Ophthalmology & Visual Science

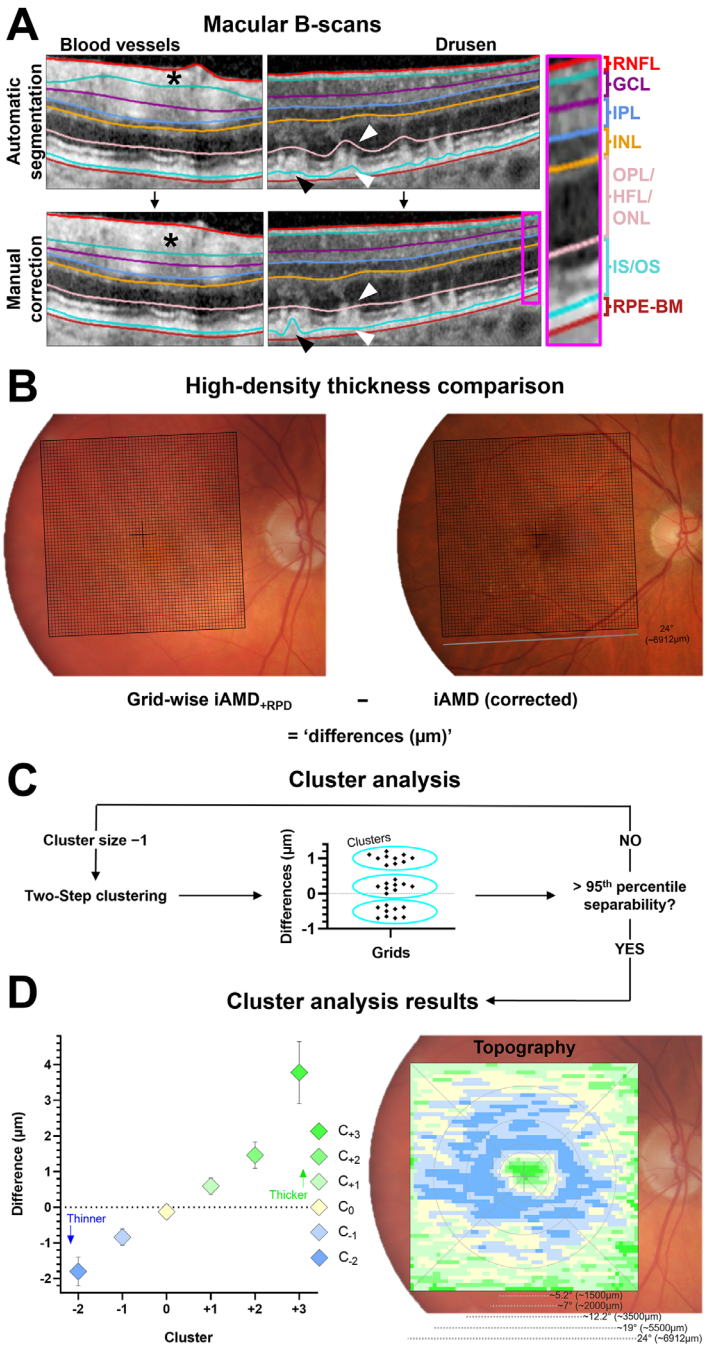

Figure 1. OCT macular cube scans were automatically segmented then manually corrected to define individual retinal layers (*pink insert*) in each B-scan using the HRA/Spectralis Viewing Module (**A**). Notable segmentation corrections included continuing through (rather than around) large vessels (*black asterisk*) and resolving mis-segmentation around conventional drusen and RPD (*black arrowhead*). In particular, the external limiting membrane was segmented to continue through RPD apices and the RPE was segmented to continue under RPD (*white arrowheads*). High-density grid thicknesses were then custom-extracted for each retinal layer across 3600 (60 × 60) grids foveally centered and covering 24 × 24 degrees or approximately 6912 × 6912 µm (**B**). Grid-wise thicknesses between $iAMD_{+RPD}$ and iAMD eyes were compared with correction for co-variables, and resultant grid-wise thickness differences simply denoted as "differences (µm)." Within each retinal layer, Two-Step clustering was applied to differences and the process re-iterated with a smaller cluster size until all clusters were separable by >95th percentile mean difference limits (**C**). Clusters were then de-convoluted to generate means [95% CI] displayed graphically (*left*), and patterns displayed topographically (*right*) (**D**). Clusters were labelled positive or negative then ranked based on magnitude of difference (µm): $C_{+1, +2, +3...}$ = increasingly thicker = darker green; $C_{-1, -2, -3...}$ = increasingly thinner = darker blue. C_0 = within 95th percentile distribution limits from zero = cream. The topography (*right*) shows an example of thickened central and peripheral macula, and thinned para-central macula. *Grey cross* denotes foveal center, *dotted grey lines* denote central macula (approximately 5.2 degrees or approximately 1500 µm diameter), peri-central macula (approximately 7 degrees or approximately 2000 µm diameter ring), para-central macula (approximately 12.2 degrees or approximately 3500 µm diameter ring), peripheral macula (approximately 19 degrees or approximately 5500 µm diameter ring), and extra-macula (outside approximately 19 degrees or approximately 5500 µm diameter). Corresponding scales *bottom right* and all images in right eye format. Note the fundus photographs are examples used for orientation purposes. Abbreviations: RNFL, retinal nerve fiber layer; GCL, ganglion cell layer; IPL, inner plexiform layer; INL, inner nuclear layer; OPL/HFL/ONL outer plexiform, Henle's fiber, and outer nuclear layers; IS/OS, inner and outer segments; RPE-BM, retinal pigment epithelium-to-Bruch's membrane.

Investigative Ophthalmology & Visual Science

right dotted grey lines). These terms were applied to each individual retinal layer excluding the RNFL due to its non-concentric distribution.[83] The RNFL was spatially delineated according to macula quadrants only, particularly as "peri-papillary/para-papillary" are not well defined.[84,85]

Statistical Analysis

Statistical analyses were performed with GraphPad Prism version 9.3.1, SPSS Version 25, and Microsoft Excel Version 2203. Statistical significance was considered as $P < 0.05$. Continuous values were expressed as mean (95% CI) unless otherwise specified. Non-continuous variables, for example, sex, presence of pigmentary abnormalities, and study group, were dummy-coded for regression analyses.[86] Normality was assessed using the D'Agostino-Pearson test. Thicknesses (by grid or cluster) were derived from each participant as a single unit of observation (i.e. independent data). Hence, single comparisons of continuous data between groups used unpaired Student's *t*-test or Mann-Whitney *U* test depending on normality. As each comparison was individually important, there was no statistical adjustment for multiple comparisons (within each individual retinal layer) and instead results were considered contextually.[87] Multiple comparisons of continuous data between groups used one-way ANOVA and Tukey's multiple comparisons test. Comparisons of continuous data within groups (i.e. between clusters within each individual retinal layer) used paired *t*-test or mixed-effects repeated measures model with non-assumption of sphericity (equal variability of differences and Geisser-Greenhouse correction) and Holm-Sidak's multiple comparisons test, depending on number of comparisons. Comparisons of categorical data used χ^2 test. Comparisons of paired proportions (i.e. between clusters subdivided into quadrants and/or central, peri-central, para-central, peripheral, and extra-macula) used McNemar's and Cochran's *Q* tests.[88] Effect sizes (Z-scores) were interpreted according to Cohen et al.[89] ≥0.2 = small, ≥0.5 = medium, and ≥0.8 = large.

Results

Participant Demographics

Single eyes from 153 individual participants were included in this study forming 3 groups: 51 with $iAMD_{+RPD}$, 51 with iAMD, and 51 normal healthy eyes. Following propensity-score matching, propensity scores (logistic regression predicted probability mean ± SD) were relatively balanced between the $iAMD_{+RPD}$ and iAMD groups (0.52 ± 0.11 and 0.48 ± 0.08, respectively), and $iAMD_{+RPD}$ and normal healthy groups (0.53 ± 0.14 and 0.47 ± 0.11, respectively). Consequently, there were no significant differences regarding age, sex, or spherical equivalent refraction between any group (Table 1). Comparison of the presence of systemic factors (i.e. diabetes mellitus, smoking, and hypertension), were also non-different between groups. Expectedly, presence of pigmentary abnormalities was different between groups, and average RPE-BM thickness was significantly greater comparing $iAMD_{+RPD}$ to iAMD ($P < 0.05$) and $iAMD_{+RPD}$ to normal ($P < 0.0001$), but not iAMD to normal ($P = 0.1$) groups. Thus, in addition to age, sex, and refraction, subsequent analyses also corrected for the presence of pigmentary abnormalities and average RPE-BM thickness.

Inner Retinal Topographical Differences Between $iAMD_{+RPD}$ and iAMD Eyes

Grid-wise thicknesses across each retinal layer were compared between $iAMD_{+RPD}$ and iAMD eyes with correction for confounding. Resultant grid-wise differences were classified into clusters, and separability confirmed between all clusters within each individual retinal layer ($P < 0.0001$ all). All between-group comparisons of cluster zero (C_0) were non-different ($P > 0.05$). To demonstrate effect sizes, differences were also converted to Z-scores using normal data.

RNFL grid-wise differences between $iAMD_{+RPD}$ and iAMD eyes were classified into three clusters (Fig. 2A). In the $iAMD_{+RPD}$ group, there was thicker RNFL (C_{+1}, +1.87 [95% CI = +0.36 to +3.39] µm, $P < 0.05$; C_{+2}, +5.89 [95% CI = +2.44 to +9.35] µm, $P < 0.01$) occupying 56.7% of the macular scan area (Fig. 2B; Table 2). Thicker RNFL was more evident at the superior than inferior (C_{+1} proportional area, 64% vs. 32%, $P < 0.01$) and nasal than temporal (C_{+1}, 55% vs. 33%, $P < 0.05$; C_{+2}, 21% vs. 0%, $P < 0.0001$; Supplementary Table S1) quadrants. The central, inferior wedge, and part superior wedge macular scan areas (43.4%) were non-different (C_0) between iAMD eyes with versus without RPD. Z-scores (SD units from normal) revealed large effect sizes in $C_{+1,+2}$ (95% CI = +1.04 to +1.28).

GCL differences between $iAMD_{+RPD}$ and iAMD eyes were assigned to two clusters (Fig. 2C). In the $iAMD_{+RPD}$ group, there was thicker GCL (C_{+1}, +2.37 [95% CI = +1.32 to +3.41] µm, $P < 0.0001$) occupying 42.4% of the macular scan area and with large effect size of +1.26 (Fig. 2D, see Table 2).

Table 1. Study Population Demographics

	$iAMD_{+RPD}$	iAMD	Normal	*P* Value
Eyes, *n*	51	51	51	–
Age, y	76.64 [74, 79.29]	74.26 [72.06, 76.46]	73.21 [71.62, 74.79]	0.08†
Sex, F:M	31:20	33:18	36:15	0.58‡
Spherical equivalent refraction, diopters	0.19 [−0.29, 0.67]	0.59 [0.05, 1.12]	0.63 [0.28, 0.98]	0.33†
Diabetes mellitus, presence:absence	7:44	7:44	4:47	0.57‡
Smoker, ever:never	7:44	9:42	4:47	0.34‡
Systemic hypertension, presence:absence	24:27	25:26	27:24	0.83‡
Pigmentary abnormalities, presence:absence	18:33	20:31	0:51	**<0.0001**‡
Average RPE-BM thickness, µm	15.56 [14.47, 16.66]	14.25 [13.53, 14.97]	13.11 [12.78, 13.45]	**<0.0001**†

Age, refraction, and RPE-BM thickness expressed as mean [95% CI].
† One-way ANOVA and ‡ χ^2 test for comparison between the three groups. Average RPE-BM thickness was significantly different comparing $iAMD_{+RPD}$ to iAMD ($P < 0.05$) and $iAMD_{+RPD}$ to normal ($P < 0.0001$), but not iAMD to normal ($P = 0.1$) groups.

Investigative Ophthalmology & Visual Science

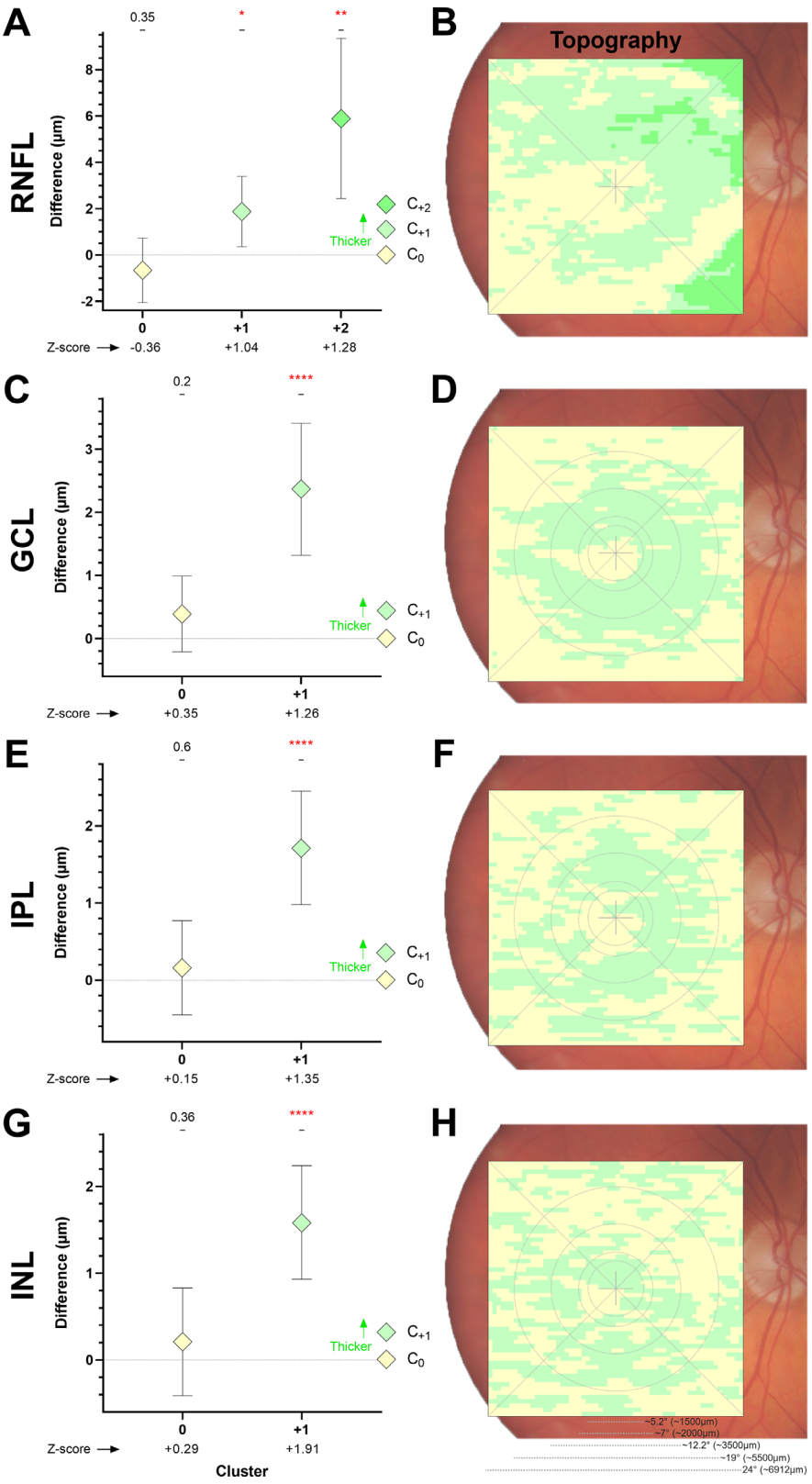

Figure 2. Retinal topography between iAMD$_{+RPD}$ and iAMD groups in the inner retina. Between-groups cluster differences presented graphically for the (**A**) RNFL, (**C**) GCL, (**E**) IPL, and (**G**) INL. Significance above each data point derived from unpaired Student's *t*-tests or Mann-Whitney *U* tests: *$P < 0.05$, **$P < 0.01$, ***$P < 0.001$, ****$P < 0.0001$. Z-scores *below* the *x*-axis. Between-groups cluster differences then presented topographically for the (**B**) RNFL, (**D**) GCL, (**F**) IPL, and (**H**) INL. *Dotted grey* lines for the RNFL denote quadrants. Presentation as in Figure 1D.

Investigative Ophthalmology & Visual Science

Table 2. Cluster Differences for $iAMD_{+RPD}$ – iAMD Eyes

			$iAMD_{+RPD}$ – iAMD	
	Clusters	Cluster sizes /3600 per layer (%)	Differences (μm)	Effect size (Z-score)
RNFL	0	1561 (43.4%)	−0.66 [−2.06, +0.73]	−0.36
	+1	1666 (46.3%)	+1.87 [+0.36, +3.39]*	+1.04
	+2	373 (10.4%)	+5.89 [+2.44, +9.35]**	+1.28
GCL	0	2075 (57.6%)	+0.39 [−0.21, +0.99]	+0.35
	+1	1525 (42.4%)	+2.37 [+1.32, +3.41]****	+1.26
IPL	0	2130 (59.2%)	+0.16 [−0.45, +0.77]	+0.15
	+1	1470 (40.8%)	+1.71 [+0.98, +2.45]****	+1.35
INL	0	2108 (58.6%)	+0.3 [−0.34, +0.94]	+0.29
	+1	1492 (41.4%)	+1.72 [+1.05, +2.39]****	+1.91
OPL/HFL/ONL	−1	989 (27.5%)	−3.21 [−5.39, −1.03]**	−1.24
	0	2611 (72.5%)	−0.47 [−2.09, +1.16]	−0.22
IS/OS	−1	759 (21.1%)	−1.67 [−2.69, −0.66]***	−3.13
	0	2841 (78.9%)	+0.12 [−0.59, +0.83]	+0.27
RPE–BM	0	2510 (69.7%)	+0.57 [−0.16, +1.29]	+0.61
	+1	1090 (30.3%)	+3.38 [+1.05, +5.71]*	+1.24

Differences expressed as mean difference [95% CI] μm. Cluster sizes expressed as grid counts /3600 per layer (%). Significance denoted by: *$P < 0.05$, **$P < 0.01$, ***$P < 0.001$, ****$P < 0.0001$.

There were no quadrant biases, although thicker GCL was most evident at the peri-central macula (C_{+1}, 93.1%, $P < 0.0001$; see Supplementary Table S1).

IPL differences were also classified into two clusters (Fig. 2E) with thicker IPL (C_{+1}, +1.71 [95% CI = +0.98 to +2.45] μm, $P < 0.0001$) occupying 40.8% macular scan area with large effect size (+1.35; Fig. 2F, see Table 2) in the $iAMD_{+RPD}$ group. There were no quadrant biases, although thicker IPL was most evident at the peri-central macula (C_{+1}, 80%, $P < 0.0001$; see Supplementary Table S1).

Finally, the INL differences were assigned to two clusters (Fig. 2G) with thicker INL (C_{+1}, +1.72 [95% CI = +1.05 to +2.39] μm, $P < 0.0001$; 41.4% macular scan area) with large effect size (+1.91; Fig. 2H, see Table 2) in the $iAMD_{+RPD}$ group. There were no quadrant biases, although thicker INL was most evident at the central macula (C_{+1}, 64%, $P < 0.05$; see Supplementary Table S1).

Outer Retinal Topographical Differences Between $iAMD_{+RPD}$ and iAMD Eyes

OPL/HFL/ONL differences between $iAMD_{+RPD}$ and iAMD eyes were classified into two clusters (Fig. 3A) with thinner OPL/HFL/ONL in the $iAMD_{+RPD}$ group (C_{-1}, −3.21 [95% CI = −5.39 to −1.03] μm, $P < 0.01$; 27.5% macular scan area) with large effect size of −1.24 (Fig. 3B, see Table 2), observed more so at the superior than inferior (C_{-1}, 58% vs. 16%, $P < 0.0001$), nasal than temporal (C_{-1}, 28% vs. 7%, $P < 0.001$) quadrants, and para-central macula (C_{-1}, 73%, $P < 0.0001$; see Supplementary Table S1).

IS/OS differences were also assigned to two clusters (Fig. 3C). There was thinner IS/OS in the $iAMD_{+RPD}$ group (C_{-1}, −1.67 [95% CI = −2.69 to −0.66] μm, $P < 0.001$) occupying 21.1% of the macular scan area with large effect size (−3.13; Fig. 3D, see Table 2). This was more evident at the temporal than nasal (C_{-1}, 44% vs. 25%, $P < 0.05$) quadrant, and para-central macula (C_{-1}, 53%, $P < 0.0001$; see Supplementary Table S1).

RPE-BM differences were classified into two clusters (see Fig. 3E) with thicker RPE-BM in the $iAMD_{+RPD}$ group covering 30.% of the macular scan area (C_{+1}, +3.38 [95% CI = +1.05 to +5.71] μm, $P < 0.05$) with large effect size of +1.24 (Fig. 3F, see Table 2). This difference extended more so at the superior than inferior (C_{+1}, 51% vs. 29%, $P < 0.05$) quadrant, and central macula (C_{+1}, 96%, $P < 0.0001$; see Supplementary Table S1).

Inner Retinal Topographical Differences Between $iAMD_{+RPD}$ and Normal Eyes

In this study, we observed inner retinal thickening of $iAMD_{+RPD}$ versus iAMD eyes, whereas previous work demonstrated inner retinal thinning of iAMD versus normal eyes.[32,35] To contextualize findings at the inner retina of $iAMD_{+RPD}$ eyes (i.e. determine whether there was more thickening or less thinning of $iAMD_{+RPD}$ from normal eyes), we repeated analyses for $iAMD_{+RPD}$ versus normal data. There was significant RNFL thinning but otherwise significant GCL, IPL, and INL thickening of $iAMD_{+RPD}$ from normal (Fig. 4, Table 3). Thus, the majority of the inner retina (except the RNFL) in $iAMD_{+RPD}$ was significantly thicker than both iAMD and normal eyes.

Discussion

High-density OCT cluster analysis of iAMD eyes with RPD versus without RPD unveiled anatomic topographical differences with large effect sizes in each retinal layer. Thicker inner retina (RNFL, GCL, IPL, and INL) in $iAMD_{+RPD}$ compared to iAMD may be related to inner retinal remodelling.[90–93] Meanwhile, thinner photoreceptor layers (OPL/HFL/ONL and IS/OS) para-centrally suggested that RPD are associated with more advanced retinal degeneration. In addition, thicker RPE-BM despite propensity-score matching for age, sex, and refraction highlighted the need for studies to correct for AMD severity when assessing RPD. These results implicate RPD as a significant associative factor to more advanced retinal degeneration in iAMD eyes at least in the para-central outer retina, and direct attention toward specific retinal areas that RPD may impact for closer clinical monitoring and future quantitative evaluation.

Partial Evidence for Inner Retinal Remodeling

The inner retinal layers (RNFL, GCL, IPL, and INL) were thicker in $iAMD_{+RPD}$ compared to iAMD eyes, consistent with other studies.[24,25,32,34,35] Our secondary analysis helped to contextualize these results and revealed significant RNFL thinning and significant GCL, IPL, and INL thickening of $iAMD_{+RPD}$ from normal eyes. Interestingly, this reaffirms recent theory that inner retinal thickening (GCL, IPL, and INL), which is "sandwiched" between contemporaneous RNFL and photoreceptor degeneration (comparing $iAMD_{+RPD}$ to normal healthy eyes), may be part of the degenerative process,[32,35] as seen with inner retinal remodeling (e.g. cellular hyperactivity and membrane hyperpermeability)[94] in other outer retinal degenerations.[90–92,95,96] A histological case study has demonstrated increased glial fibrillary acidic protein expression – a marker of retinal glial stress[92] – at the inner retina overlying RPD,[4] although to our knowledge no strong evidence of inner retinal remodeling associated with RPD has yet been reported. Our findings

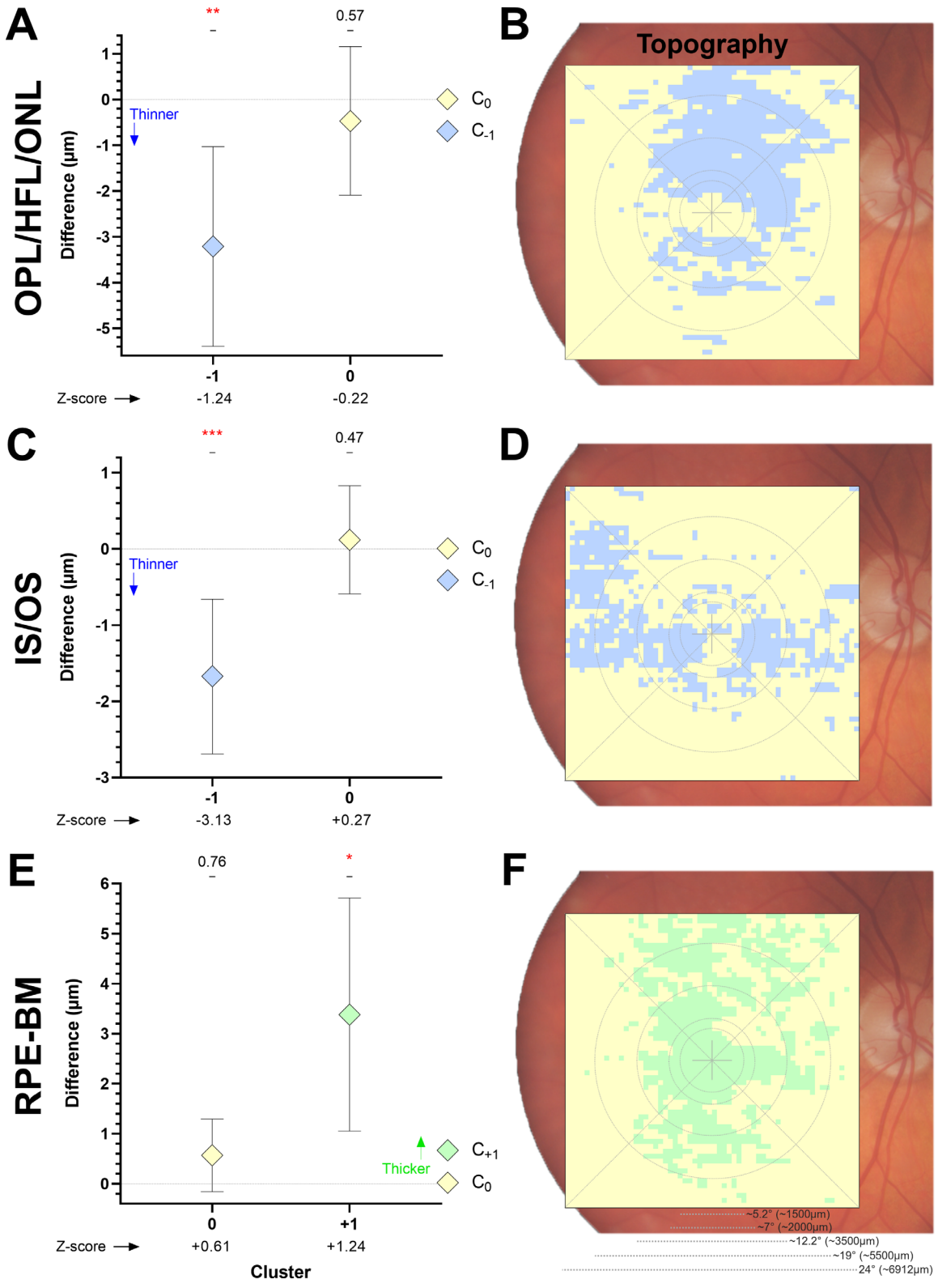

Figure 3. Retinal topography between iAMD$_{+RPD}$ and iAMD groups in the outer retina. Between-groups cluster differences presented graphically for the (**A**) OPL/HFL/ONL, (**C**) IS/OS, and (**E**) RPE-BM, and topographically for the (**B**) OPL/HFL/ONL, (**D**) IS/OS, and (**F**) RPE-BM. Presentation as in Figure 2.

of peri-central inner retinal thickening when comparing iAMD$_{+RPD}$ to both iAMD and normal healthy eyes aligns with the greater density of inner retinal cells including ganglion cells,[97] bipolar cells, horizontal cells, amacrine cells, and Müller cells,[98,99] although further study is required to explore inner retinal changes associated with RPD.

Investigative Ophthalmology & Visual Science

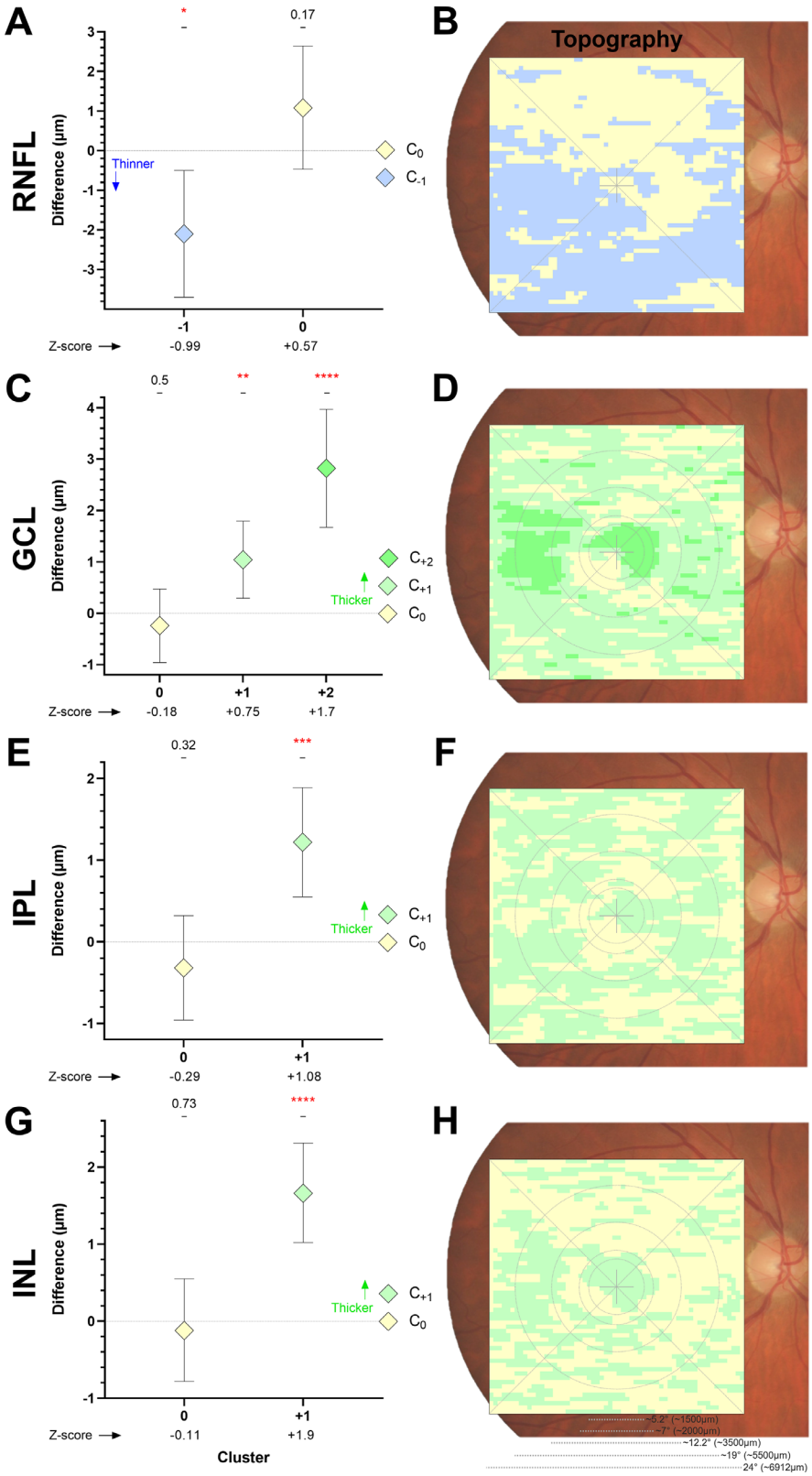

Figure 4. Retinal topography between iAMD$_{+RPD}$ and normal groups in the inner retina. Between-groups cluster differences presented graphically for the (**A**) RNFL, (**C**) GCL, (**E**) IPL, and (**G**) INL, and topographically for the (**B**) RNFL, (**D**) GCL, (**F**) IPL, and (**H**) INL. Presentation as in Figure 2.

Investigative Ophthalmology & Visual Science

Table 3. Cluster Differences for $iAMD_{+RPD}$ – Normal Eyes at the Inner Retina

			$iAMD_{+RPD}$ – normal	
	Clusters	Cluster sizes /3600 per layer (%)	Differences (μm)	Effect size (Z-score)
RNFL	−1	1801 (50%)	−2.1 [−3.7, −0.5]*	−0.99
	0	1799 (50%)	+1.08 [−0.47, +2.64]	+0.57
GCL	0	1077 (29.9%)	−0.24 [−0.96, +0.47]	−0.18
	+1	2064 (57.3%)	+1.04 [+0.29, +1.79]**	+0.75
	+2	459 (12.8%)	+2.82 [+1.67, +3.97]****	+1.7
IPL	0	1584 (44%)	−0.32 [−0.96, +0.32]	−0.29
	+1	2016 (56%)	+1.22 [+0.55, +1.89]***	+1.08
INL	0	2252 (62.6%)	−0.12 [−0.78, +0.55]	−0.11
	+1	1348 (37.4%)	+1.66 [+1.02, +2.31]****	+1.9

Differences expressed as mean difference [95% CI] μm. Cluster sizes expressed as grid counts /3600 per layer (%). Significance denoted by: *$P < 0.05$, **$P < 0.01$, ***$P < 0.001$, ****$P < 0.0001$.

Furthermore, why the inner retina may be altered in a primarily outer retinal disease is yet unknown. Previously, we considered the possibility of anterograde trans-synaptic degeneration,[100,101] but could not observe any significant relationships for OCT thickness changes between the outer and inner retinal layers in early/iAMD.[35] Alternatively, there are suggestions that the outer and inner retinal layers in AMD may be linked via common inflammatory[102–105] and/or vascular pathways,[106–114] such as the choroid.[114] Such theories could explain why AMD prevalence is greater in patients with glaucoma, for example, despite controlling for related variables such as age and sex.[115–117]

RPD Are Associated With More Advanced Outer Retinal Degeneration

Recently, we found para-central photoreceptor thinning in early/iAMD compared to normal eyes,[32,35] which corresponds to rod susceptibility in AMD[98,118,119] seen via structural[120–126] and functional[127–130] measures. In this study, the RPD phenotype of iAMD presented with even greater photoreceptor thinning para-centrally, suggesting even greater rod susceptibility. These differences were unlikely to be an artifact of mechanical compression from underlying drusen as for each layer (except the RPE-BM), we corrected for differences in RPE-BM thickness between groups. Our previous study also confirmed photoreceptor thinning began at the early stage of AMD, prior to significant thickening of the RPE-BM.[35] Photoreceptor thinning was concordant with the overwhelming number of studies demonstrating that RPD are associated with increased risk of progression to late AMD.[6–10,20,131–142] Subanalyses highlighted that this para-central thinning was more prevalent superiorly in the OPL/HFL/ONL aligning with greater superior macula distribution of RPD[2,143,144] and/or rods.[118,119] The temporal bias of thinning in the IS/OS, however, remains enigmatic.

Our propensity-score matched sample (matching age, sex, and refraction) also underscored the importance of correcting for AMD severity when assessing RPD. When considering studies that have made the correction for AMD severity, evidence for[6–10] and against[11–14] RPD as a risk factor for AMD progression is more equally divided. Nonetheless, several studies, including this one, suggest that RPD is associated with more advanced outer retinal degeneration in AMD eyes.[24–29] Clinicians should consider closer monitoring of patients with iAMD with RPD and, in the future, quantitative evaluation of photoreceptor thicknesses may be utilized to monitor retinal integrity.

Limitations

The primary limitation of this study is the use of cross-sectional OCT data, which does not identify specific cellular and synaptic changes nor their temporality (i.e. do RPD cause macular anatomic changes or are patients with specific macular anatomy more susceptible to developing RPD?). The latter theory has garnered increasing attention as recent studies confirm various AMD genotypes influence phenotypic expressions, such as retinal layer thicknesses[145–147] even prior to the development of AMD.[148] Regardless of the chronology of events, the association of RPD with more advanced para-central outer retinal degeneration remains a relevant consideration for closer monitoring of patients with iAMD.

The small magnitude (μm) of our results may also have limited immediate clinical translatability considering the higher magnitude test-retest variability of commercial OCT devices,[149] which also typically do not enable photoreceptor thickness analysis. Our large effect sizes, however, suggests future clinical utility as advancing OCT technology lessens test-retest variability and enables thickness analyses of more individual retinal layers. Longitudinal data with other structural and visual function testing modalities will also elucidate specific macula anatomical changes that may not be measurable via thickness alone (e.g. disrupted photoreceptor IS ellipsoid integrity), and expound their cause-and-effect inter-relationship with RPD.

Finally, lack of universal definition and quantification methods for RPD (including subtypes)[150] meant that direct comparability of our results to other studies' is difficult, as exampled above when interpreting whether RPD is[6–9,20,131–142] or is not[11–14] a risk factor for AMD progression. To mitigate this, we used a well-established definition for the number of lesions (≥5) and imaging modality (OCT) required for RPD diagnosis,[49] whereby OCT demonstrates excellent sensitivity and specificity.[151–154] Future consensus on RPD definition and quantification will facilitate exploration of any dose-response relationship between RPD severity and retinal thickness changes.

Conclusion

Anatomic topographical differences with large effect sizes in each retinal layer were observed between iAMD eyes with RPD versus without RPD. Thinner photoreceptor layers suggested RPD are associated with more advanced retinal degeneration at least in the para-central outer retina. Thicker inner retinal layers were also observed but their pathologic meaning requires further study. These results suggest that clinicians should consider closer monitoring of patients with iAMD when RPD are present. In the future, quantitative evaluation of photoreceptor thicknesses may also help clinicians monitor the potential deleterious effects of RPD on retinal integrity.

Acknowledgments

Supported, in part, by the National Health and Medical Research Council of Australia (NHMRC) grant #1186915 to M.K. and

Investigative Ophthalmology & Visual Science

D.A.C., and NHMRC grant #1174385 to L.N.S. M.T. and N.E. are supported by the Australian Research Training Program scholarship. Guide Dogs NSW/ACT provides support for the Centre for Eye Health (the clinic of recruitment).

Disclosure: **M. Trinh**, None; **N. Eshow**, None; **D. Alonso-Caneiro**, None; **M. Kalloniatis**, None; **L. Nivison-Smith**, None

References

1. Zweifel SA, Spaide RF, Curcio CA, Malek G, Imamura Y. Reticular pseudodrusen are subretinal drusenoid deposits. *Ophthalmology*. 2010;117:303–312.e1.
2. Curcio CA, Messinger JD, Sloan KR, McGwin G, Medeiros NE, Spaide RF. Subretinal drusenoid deposits in non-neovascular age-related macular degeneration: morphology, prevalence, topography, and biogenesis model. *Retina*. 2013;33:265–276.
3. Chen L, Messinger JD, Zhang Y, Spaide RF, Freund KB, Curcio CA. Subretinal drusenoid deposit in age-related macular degeneration: histologic insights into initiation, progression to atrophy, and imaging. *Retina Phila Pa*. 2020;40:618–631.
4. Greferath U, Guymer RH, Vessey KA, Brassington K, Fletcher EL. Correlation of histologic features with in vivo imaging of reticular pseudodrusen. *Ophthalmology*. 2016;123:1320–1331.
5. Rudolf M, Malek G, Messsinger JD, Clark ME, Wang L, Curcio CA. Sub-retinal drusenoid deposits in human retina: organization and composition. *Exp Eye Res*. 2008;87:402–408.
6. Nassisi M, Lei J, Abdelfattah NS, et al. OCT risk factors for development of late age-related macular degeneration in the fellow eyes of patients enrolled in the HARBOR study. *Ophthalmology*. 2019;126:1667–1674.
7. Domalpally A, Agrón E, Pak JW, et al. Prevalence, risk, and genetic association of reticular pseudodrusen in age-related macular degeneration: Age-Related Eye Disease Study 2 report 21. *Ophthalmology*. 2019;126:1659–1666.
8. Zhou Q, Daniel E, Maguire MG, et al. Pseudodrusen and incidence of late age-related macular degeneration in fellow eyes in the comparison of age-related macular degeneration treatments trials. *Ophthalmology*. 2016;123:1530–1540.
9. Finger RP, Chong E, McGuinness MB, et al. Reticular pseudodrusen and their association with age-related macular degeneration: the Melbourne collaborative cohort study. *Ophthalmology*. 2016;123:599–608.
10. Agrón E, Domalpally A, Cukras CA, et al. Reticular pseudodrusen: the third macular risk feature for progression to late age-related macular degeneration. *Ophthalmology*. 2022;129(10):1107–1119.
11. Finger RP, Wu Z, Luu CD, et al. Reticular pseudodrusen: a risk factor for geographic atrophy in fellow eyes of individuals with unilateral choroidal neovascularization. *Ophthalmology*. 2014;121:1252–1256.
12. Sleiman K, Veerappan M, Winter KP, et al. Optical coherence tomography predictors of risk for progression to non-neovascular atrophic age-related macular degeneration. *Ophthalmology*. 2017;124:1764–1777.
13. Wu Z, Kumar H, Hodgson LAB, Guymer RH. Reticular pseudodrusen on the risk of progression in intermediate age-related macular degeneration. *Am J Ophthalmol*. 2022;239:202–211.
14. Thiele S, Nadal J, Pfau M, et al. Prognostic value of retinal layers in comparison with other risk factors for conversion of intermediate age-related macular degeneration. *Ophthalmol Retina*. 2020;4:31–40.
15. Marsiglia M, Boddu S, Bearelly S, et al. Association between geographic atrophy progression and reticular pseudodrusen in eyes with dry age-related macular degeneration. *Invest Ophthalmol Vis Sci*. 2013;54:7362–7369.
16. Mantel I, Dirani A, Zola M, Parvin P, De Massougnes S, Bergin C. Macular atrophy incidence in anti-vascular endothelial growth factor-treated neovascular age-related macular degeneration: risk factor evaluation for individualized treatment need of Ranibizumab or Aflibercept according to an observe-and-plan regimen. *Retina Phila Pa*. 2019;39:906–917.
17. Guymer RH, Wu Z, Hodgson LAB, et al. Subthreshold nanosecond laser intervention in age-related macular degeneration: the LEAD randomized controlled clinical trial. *Ophthalmology*. 2019;126:829–838.
18. Wu Z, Fletcher EL, Kumar H, Greferath U, Guymer RH. Reticular pseudodrusen: a critical phenotype in age-related macular degeneration. *Prog Retin Eye Res*. 2022;88:101017.
19. Chiang TT-K, Keenan TD, Agrón E, et al. Macular thickness in intermediate age-related macular degeneration is influenced by disease severity and subretinal drusenoid deposit presence. *Invest Ophthalmol Vis Sci*. 2020;61:59.
20. Hogg RE, Silva R, Staurenghi G, et al. Clinical characteristics of reticular pseudodrusen in the fellow eye of patients with unilateral neovascular age-related macular degeneration. *Ophthalmology*. 2014;121:1748–1755.
21. Ahn SM, Lee SY, Hwang S-Y, Kim S-W, Oh J, Yun C. Retinal vascular flow and choroidal thickness in eyes with early age-related macular degeneration with reticular pseudodrusen. *BMC Ophthalmol*. 2018;18:184.
22. Garg A, Oll M, Yzer S, et al. Reticular pseudodrusen in early age-related macular degeneration are associated with choroidal thinning. *Invest Ophthalmol Vis Sci*. 2013;54:7075–7081.
23. Nittala MG, Hogg RE, Luo Y, et al. Changes in retinal layer thickness in the contralateral eye of patients with unilateral neovascular age-related macular degeneration. *Ophthalmol Retina*. 2019;3:112–121.
24. Sassmannshausen M, Pfau M, Thiele S, et al. Longitudinal Analysis of Structural and Functional Changes in Presence of Reticular Pseudodrusen Associated With Age-Related Macular Degeneration. *Invest Ophthalmol Vis Sci*. 2020;61:19.
25. Farinha C, Silva AL, Coimbra R, et al. Retinal layer thicknesses and neurodegeneration in early age-related macular degeneration: insights from the Coimbra Eye Study. *Graefes Arch Clin Exp Ophthalmol Albrecht Von Graefes Arch Klin Exp Ophthalmol*. 2021;259:2545–2557.
26. Sevilla MB, McGwin G, Lad EM, et al. Relating retinal morphology and function in aging and early to intermediate age-related macular degeneration subjects. *Am J Ophthalmol*. 2016;165:65–77.
27. Ramon C, Cardona G, Biarnés M, Ferraro LL, Monés J. Longitudinal changes in outer nuclear layer thickness in soft drusen and reticular pseudodrusen. *Clin Exp Optom*. 2019;102:601–610.
28. Camacho P, Dutra-Medeiros M, Cabral D, Silva R. Outer retina and choroidal thickness in intermediate age-related macular degeneration: reticular pseudodrusen findings. *Ophthalmic Res*. 2018;59:212–220.
29. Jang S, Park SY, Ahn SM, et al. Morphologic features of the retinal pigment epithelium and associated chorioretinal characteristics in eyes with early age-related macular degeneration and subretinal drusenoid deposits. *Retina Phila Pa*. 2020;40:686–694.
30. Wong DWS. The Modifiable Areal Unit Problem (MAUP). In: Janelle DG, Warf B, Hansen K , eds. *Worldminds: geographical perspectives on 100 problems: commemorating the 100th anniversary of the Association of American*

Geographers 1904–2004. Netherlands: Springer; 2004:571–575.
31. Jelinski DE, Wu J. The modifiable areal unit problem and implications for landscape ecology. *Landsc Ecol*. 1996;11:129–140.
32. Trinh M, Khou V, Kalloniatis M, Nivison-Smith L. Location-specific thickness patterns in intermediate age-related macular degeneration reveals anatomical differences in multiple retinal layers. *Invest Ophthalmol Vis Sci*. 2021;62:13.
33. Trinh M, Khou V, Zangerl B, Kalloniatis M, Nivison-Smith L. Modelling normal age-related changes in individual retinal layers using location-specific OCT analysis. *Sci Rep*. 2021;11:558.
34. Trinh M, Tong J, Yoshioka N, Zangerl B, Kalloniatis M, Nivison-Smith L. Macula ganglion cell thickness changes display location-specific variation patterns in intermediate age-related macular degeneration. *Invest Ophthalmol Vis Sci*. 2020;61:2.
35. Trinh M, Kalloniatis M, Alonso-Caneiro D, Nivison-Smith L. High-density optical coherence tomography analysis provides insights into early/intermediate age-related macular degeneration retinal layer changes. *Invest Ophthalmol Vis Sci*. 2022;63:36.
36. Trinh M, Kalloniatis M, Nivison-Smith L. Radial Peripapillary Capillary Plexus Sparing and Underlying Retinal Vascular Impairment in Intermediate Age-Related Macular Degeneration. *Invest Ophthalmol Vis Sci*. 2021;62:2.
37. Wang H, Kalloniatis M. Clinical outcomes of the Centre for Eye Health: an intra-professional optometry-led collaborative eye care clinic in Australia. *Clin Exp Optom*. 2021;104:795–804.
38. Chen X, Nie C, Gong Y, et al. Peripapillary retinal nerve fiber layer changes in preclinical diabetic retinopathy: a meta-analysis. *PLoS One*. 2015;10:e0125919.
39. Yang T-K, Huang X-G, Yao J-Y. Effects of cigarette smoking on retinal and choroidal thickness: a systematic review and meta-analysis. *J Ophthalmol*. 2019;2019:8079127.
40. Mauschitz MM, Bonnemaijer PWM, Diers K, et al. Systemic and ocular determinants of peripapillary retinal nerve fiber layer thickness measurements in the European eye epidemiology (E3) population. *Ophthalmology*. 2018;125:1526–1536.
41. Bressler NM, Edwards AR, Antoszyk AN, et al. Retinal thickness on Stratus optical coherence tomography in people with diabetes and minimal or no diabetic retinopathy. *Am J Ophthalmol*. 2008;145:894–901.
42. Niestrata-Ortiz M, Fichna P, Stankiewicz W, Stopa M. Determining the effect of diabetes duration on retinal and choroidal thicknesses in children with type 1 diabetes mellitus. *Retina Phila Pa*. 2020;40:421–427.
43. Demir M, Oba E, Sensoz H, Ozdal E. Retinal nerve fiber layer and ganglion cell complex thickness in patients with type 2 diabetes mellitus. *Indian J Ophthalmol*. 2014;62:719–720.
44. Lee WH, Lee M-W, Lim H-B, et al. Retinal nerve fibre layer/ganglion cell-inner plexiform layer thickness ratio in patients with systemic hypertension. *Acta Ophthalmol (Copenh)*. 2022;100:e150–e156.
45. Duman R, Duman R, Sabaner MC, Çetinkaya E. Effect of smoking on the thickness of retinal layers in healthy smokers. *Cutan Ocul Toxicol*. 2017;36:366–369.
46. Dervişoğulları MS, Totan Y, Tenlik A, Yuce A. Effects of cigarette smoking on choroidal and retinal thickness and ocular pulse amplitude. *Cutan Ocul Toxicol*. 2015;34:217–221.
47. Lloyd-Jones DM, Evans JC, Levy D. Hypertension in adults across the age spectrum: current outcomes and control in the community. *JAMA*. 2005;294:466–472.
48. Cheng YJ, Imperatore G, Geiss LS, et al. Secular changes in the age-specific prevalence of diabetes among U.S. adults: 1988-2010. *Diabetes Care*. 2013;36:2690–2696.
49. Ueda-Arakawa N, OOto S, Tsujikawa A, Yamashiro K, Oishi A, Yoshimura N. Sensitivity and specificity of detecting reticular pseudodrusen in multimodal imaging in Japanese patients. *Retina Phila Pa*. 2013;33:490–497.
50. Ferris FL, Wilkinson CP, Bird A, et al. Clinical classification of age-related macular degeneration. *Ophthalmology*. 2013;120:844–851.
51. Hallak JA, de Sisternes L, Osborne A, Yaspan B, Rubin DL, Leng T. Imaging, genetic, and demographic factors associated with conversion to neovascular age-related macular degeneration: secondary analysis of a randomized clinical trial. *JAMA Ophthalmol*. 2019;137:738–744.
52. Waldstein SM, Vogl WD, Bogunovic H, Sadeghipour A, Riedl S, Schmidt-Erfurth U. Characterization of drusen and hyperreflective foci as biomarkers for disease progression in age-related macular degeneration using artificial intelligence in optical coherence tomography. *JAMA Ophthalmol*. 2020;138:740–747.
53. Guymer RH, Baird PN, Varsamidis M, et al. Proof of concept, randomized, placebo-controlled study of the effect of Simvastatin on the course of age-related macular degeneration. *PLoS One*. 2013;8:e83759.
54. Salvi SM, Akhtar S, Currie Z. Ageing changes in the eye. *Postgrad Med J*. 2006;82:581–587.
55. Wang JJ, Foran S, Mitchell P. Age-specific prevalence and causes of bilateral and unilateral visual impairment in older Australians: the Blue Mountains Eye Study. *Clin Experiment Ophthalmol*. 2000;28:268–273.
56. US Preventive Services Task Force. Screening for impaired visual acuity in older adults: US preventive services task force recommendation statement. *JAMA*. 2022;327:2123–2128.
57. Pitts DG. Visual acuity as a function of age. *J Am Optom Assoc*. 1982;53:117–124.
58. Rosenbaum PR, Rubin DB. Constructing a control group using multivariate matched sampling methods that incorporate the propensity score. *Am Stat*. 1985;39:33–38.
59. Stuart EA. Matching methods for causal inference: A review and a look forward. *Stat Sci Rev J Inst Math Stat*. 2010;25:1–21.
60. Lunt M. Selecting an appropriate caliper can be essential for achieving good balance with propensity score matching. *Am J Epidemiol*. 2014;179:226–235.
61. Drasdo N, Fowler CW. Non-linear projection of the retinal image in a wide-angle schematic eye. *Br J Ophthalmol*. 1974;58:709–714.
62. Heidelberg Engineering GmbH. Spectralis product family user manual software version 6.7. 2016. Available at: https://docplayer.net/140463196-Spectralis-glaucoma-module-premium-edition-user-manual-software-version-6-7-november-2016-heidelberg-engineering-gmbh-article-no-int.html.
63. Kolb H. Facts and figures concerning the human retina. In: Kolb H, Fernandez E, Nelson R , eds. *Webvision: The Organization of the Retina and Visual System*. University of Utah Health Sciences Center; 1995.
64. Lujan BJ, Roorda A, Knighton RW, Carroll J. Revealing Henle's fiber layer using spectral domain optical coherence tomography. *Invest Ophthalmol Vis Sci*. 2011;52:1486–1492.
65. Saxena S, Srivastav K, Cheung CM, Ng JY, Lai TY. Photoreceptor inner segment ellipsoid band integrity on spectral domain optical coherence tomography. *Clin Ophthalmol Auckl NZ*. 2014;8:2507–2522.

Investigative Ophthalmology & Visual Science

66. Tian J, Varga B, Tatrai E, et al. Performance evaluation of automated segmentation software on optical coherence tomography volume data. *J Biophotonics*. 2016;9:478–489.
67. Maloca PM, Lee AY, de Carvalho ER, et al. Validation of automated artificial intelligence segmentation of optical coherence tomography images. *PLoS One*. 2019;14:e0220063.
68. de Azevedo AGB, Takitani GEDS, Godoy BR, et al. Impact of manual correction over automated segmentation of spectral domain optical coherence tomography. *Int J Retina Vitr*. 2020;6:4.
69. Camacho P, Dutra-Medeiros M, Salgueiro L, Sadio S, Rosa PC. Manual segmentation of 12 layers of the retina and choroid through SD-OCT in intermediate AMD: repeatability and reproducibility. *J Ophthalmic Vis Res JOVR*. 2021;16(3):384–392.
70. Querques G, Canouï-Poitrine F, Coscas F, et al. Analysis of progression of reticular pseudodrusen by spectral domain–optical coherence tomography. *Invest Ophthalmol Vis Sci*. 2012;53:1264–1270.
71. Tong J, Alonso-Caneiro D, Yoshioka N, Kalloniatis M, Zangerl B. Custom extraction of macular ganglion cell-inner plexiform layer thickness more precisely co-localizes structural measurements with visual fields test grids. *Sci Rep*. 2020;10:18527.
72. Tsang SH, Sharma T. Retinal histology and anatomical landmarks. *Adv Exp Med Biol*. 2018;1085:3–5.
73. Gaurisankar ZS, van Rijn GA, Lima JEE, et al. Correlations between ocular biometrics and refractive error: a systematic review and meta-analysis. *Acta Ophthalmol (Copenh)*. 2019;97:735–743.
74. Parthasarathy MK, Bhende M. Effect of ocular magnification on macular measurements made using spectral domain optical coherence tomography. *Indian J Ophthalmol*. 2015;63:427–431.
75. Bille JF , ed. *High Resolution Imaging in Microscopy and Ophthalmology: New Frontiers in Biomedical Optics*. New York, NY: Springer; 2019.
76. Frades I, Matthiesen R. Overview on techniques in cluster analysis. *Methods Mol Biol Clifton NJ*. 2010;593:81–107.
77. Gelbard R, Goldman O, Spiegler I. Investigating diversity of clustering methods: an empirical comparison. *Data Knowl Eng*. 2007;63:155–166.
78. Vichi M. *Data science: innovative developments in data analysis and clustering*. New York, NY: Springer; 2017.
79. Raykov YP, Boukouvalas A, Baig F, Little MA. What to do when k-means clustering fails: a simple yet principled alternative algorithm. *PLoS One*. 2016;11:e0162259.
80. Bacher J, Wenzig K, Vogler M. SPSS Twostep Cluster – a first evaluation. *Work and discussion paper*. Friedrich-Alexander-Universität Erlangen-Nürnberg, Lehrstuhl für Soziologie; 2004. Available at: https://www.researchgate.net/publication/215665884_SPSS_TwoStep_Cluster_-_a_first_evaluation.
81. Payton ME, Greenstone MH, Schenker N. Overlapping confidence intervals or standard error intervals: what do they mean in terms of statistical significance? *J Insect Sci*. 2003;3:34.
82. Austin PC, Hux JE. A brief note on overlapping confidence intervals. *J Vasc Surg*. 2002;36:194–195.
83. Varma R, Skaf M, Barron E. Retinal nerve fiber layer thickness in normal human eyes. *Ophthalmology*. 1996;103:2114–2119.
84. Van Buskirk EM. Peripheral paraphrasing the glaucoma lexicon. *J Glaucoma*. 1999;8:157–158.
85. MacLeod JD. 'Parapapillary' versus 'peripapillary'. *J Glaucoma*. 1999;8:342.
86. Polissar L, Diehr P. Regression analysis in health services research: the use of dummy variables. *Med Care*. 1982;20:959–966.
87. Armstrong RA. When to use the Bonferroni correction. *Ophthalmic Physiol Opt J Br Coll Ophthalmic Opt Optom*. 2014;34:502–508.
88. Hazra A, Gogtay N. Biostatistics series module 4: Comparing groups - categorical variables. *Indian J Dermatol*. 2016;61:385.
89. Cohen J. *Statistical power analysis for the behavioural sciences*. Mahwah, NJ: Lawrence Erlbaum Associates; 1988.
90. Johnson PT, et al. Drusen-associated degeneration in the retina. *Invest Ophthalmol Vis Sci*. 2003;44:4481–4488.
91. Madigan MC, Penfold PL, Provis JM, Balind TK, Billson FA. Intermediate filament expression in human retinal macroglia. Histopathologic changes associated with age-related macular degeneration. *Retina Phila Pa*. 1994;14:65–74.
92. Wu KHC, Madigan MC, Billson FA, Penfold PL. Differential expression of GFAP in early v late AMD: a quantitative analysis. *Br J Ophthalmol*. 2003;87:1159–1166.
93. Chua J, Nivison-Smith L, Fletcher EL, Trenholm S, Awatramani GB, Kalloniatis M. Early remodelling of Müller cells in the rd/rd mouse model of retinal dystrophy: Müller cells in rd/rd mouse retina. *J Comp Neurol*. 2013;521:2439–2453.
94. Telias M, Nawy S, Kramer RH. Degeneration-dependent retinal remodeling: looking for the molecular trigger. *Front Neurosci*. 2020;14:1347.
95. Sullivan RKP, WoldeMussie E, Pow DV. Dendritic and synaptic plasticity of neurons in the human age-related macular degeneration retina. *Invest Ophthalmol Vis Sci*. 2007;48:2782–2791.
96. Fariss RN, Li Z-Y, Milam AH. Abnormalities in rod photoreceptors, amacrine cells, and horizontal cells in human retinas with retinitis pigmentosa. *Am J Ophthalmol*. 2000;129:215–223.
97. Curcio CA, Allen KA. Topography of ganglion cells in human retina. *J Comp Neurol*. 1990;300:5–25.
98. Lee SCS, Martin PR, Grünert U. Topography of neurons in the rod pathway of human retina. *Invest Ophthalmol Vis Sci*. 2019;60:2848–2859.
99. Masri RA, Weltzien F, Purushothuman S, Lee SCS, Martin PR, Grünert U. Composition of the inner nuclear layer in human retina. *Invest Ophthalmol Vis Sci*. 2021;62:22.
100. Feigl B, Brown B, Lovie-Kitchin J, Swann P. Functional loss in early age-related maculopathy: the ischaemia postreceptoral hypothesis. *Eye*. 2007;21:689–696.
101. Panneman EL, Coric D, Tran LMD, de Vries-Knoppert WAEJ, Petzold A. Progression of anterograde trans-synaptic degeneration in the human retina is modulated by axonal convergence and divergence. *Neuro-Ophthalmol*. 2019;43:382–390.
102. Kauppinen A, Paterno JJ, Blasiak J, Salminen A, Kaarniranta K. Inflammation and its role in age-related macular degeneration. *Cell Mol Life Sci*. 2016;73:1765–1786.
103. Litwińska Z, Sobuś A, Łuczkowska K, et al. The interplay between systemic inflammatory factors and microRNAs in age-related macular degeneration. *Front Aging Neurosci*. 2019;11:286.
104. Ozaki E, Campbell M, Kiang AS, Humphries M, Doyle SL, Humphries P. Inflammation in age-related macular degeneration. *Adv Exp Med Biol*. 2014;801:229–235.
105. Cheung CMG, Wong TY. Is age-related macular degeneration a manifestation of systemic disease? New prospects for early intervention and treatment. *J Intern Med*. 2014;276:140–153.

Investigative Ophthalmology & Visual Science

106. Velaga SB, Nittala MG, Vupparaboina KK, et al. Choroidal vascularity index and choroidal thickness in eyes with reticular pseudodrusen. *Retina Phila Pa*. 2020;40:612–617.
107. Rosa R, Corazza P, Musolino M, et al. Choroidal changes in intermediate age-related macular degeneration patients with drusen or pseudodrusen. *Eur J Ophthalmol*. 2021;31:505–513.
108. Viggiano P, Toto L, Ferro G, Evangelista F, Porreca A, Mastropasqua R. Choroidal structural changes in different intermediate AMD patterns. *Eur J Ophthalmol*. 2022;32:460–467.
109. Temel E, Batioğlu F, Demirel S, Özcan G, Yanik Ö, Özmert E. Vascular and structural alterations of the choroid evaluated by optical coherence tomography angiography and enhanced-depth imaging optical coherence tomography in eyes with reticular pseudodrusen and soft drusen. *Photodiagnosis Photodyn Ther*. 2021;36:102549.
110. Sacconi R, Vella G, Battista M, et al. Choroidal vascularity index in different cohorts of dry age-related macular degeneration. *Transl Vis Sci Technol*. 2021;10:26.
111. Yun C, Oh J, Ahn SE, Hwang SY, Kim SW, Huh K. Peripapillary choroidal thickness in patients with early age-related macular degeneration and reticular pseudodrusen. *Graefes Arch Clin Exp Ophthalmol Albrecht Von Graefes Arch Klin Exp Ophthalmol*. 2016;254:427–435.
112. Kumar V. Reticular pseudodrusen and thin choroid are associated with angioid streaks. *Ophthalmic Surg Lasers Imaging Retina*. 2018;49:402–408.
113. Mano F, Sprehe N, Olsen TW. Association of drusen phenotype in age-related macular degeneration from human eye-bank eyes to disease stage and cause of death. *Ophthalmol Retina*. 2021;5:743–749.
114. Garg A, Blumberg DM, Al-Aswad LA, et al. Associations between β-peripapillary atrophy and reticular pseudodrusen in early age-related macular degeneration. *Invest Ophthalmol Vis Sci*. 2017;58:2810–2815.
115. Griffith JF, Goldberg JL. Prevalence of comorbid retinal disease in patients with glaucoma at an academic medical center. *Clin Ophthalmol Auckl NZ*. 2015;9:1275–1284.
116. Zlateva GP, Javitt JC, Shah SN, Zhou Z, Murphy JG. Comparison of comorbid conditions between neovascular age-related macular degeneration patients and a control cohort in the Medicare population. *Retina Phila Pa*. 2007;27:1292–1299.
117. Hu C-C, Ho J-D, Lin H-C, Kao L-T. Association between open-angle glaucoma and neovascular age-related macular degeneration: a case-control study. *Eye Lond Engl*. 2017;31:872–877.
118. Ahnelt PK. The photoreceptor mosaic. *Eye Lond Engl*. 1998;12(Pt 3b):531–540.
119. Curcio CA, Sloan KR, Kalina RE, Hendrickson AE. Human photoreceptor topography. *J Comp Neurol*. 1990;292:497–523.
120. Godara P, Siebe C, Rha J, Michaelides M, Carroll J. Assessing the photoreceptor mosaic over drusen using adaptive optics and SD-OCT. *Ophthalmic Surg Lasers Imaging Off J Int Soc Imaging Eye*. 2010;41(Suppl):S104–S108.
121. Mrejen S, Sato T, Curcio CA, Spaide RF. Assessing the cone photoreceptor mosaic in eyes with pseudodrusen and soft drusen in vivo using adaptive optics imaging. *Ophthalmology*. 2014;121:545–551.
122. Reumueller A, Schmidt-Erfurth U, Salas M, et al. Three-dimensional adaptive optics–assisted visualization of photoreceptors in healthy and pathologically aged eyes. *Invest Ophthalmol Vis Sci*. 2019;60:1144–1155.
123. Querques G, Kamami-Levy C, Blanco-Garavito R, et al. Appearance of medium–large drusen and reticular pseudodrusen on adaptive optics in age-related macular degeneration. *Br J Ophthalmol*. 2014;98:1522–1527.
124. Zayit-Soudry S, Duncan JL, Syed R, Menghini M, Roorda AJ. Cone structure imaged with adaptive optics scanning laser ophthalmoscopy in eyes with nonneovascular age-related macular degeneration. *Invest Ophthalmol Vis Sci*. 2013;54:7498–7509.
125. Boretsky A, Khan F, Burnett G, et al. In vivo imaging of photoreceptor disruption associated with age-related macular degeneration: a pilot study. *Lasers Surg Med*. 2012;44:603–610.
126. Curcio CA, Medeiros NE, Millican CL. Photoreceptor loss in age-related macular degeneration. *Invest Ophthalmol Vis Sci*. 1996;37:1236–1249.
127. Flamendorf J, Agrón E, Wong WT, et al. Impairments in dark adaptation are associated with age-related macular degeneration severity and reticular pseudodrusen. *Ophthalmology*. 2015;122:2053–2062.
128. Owsley C, McGwin G, Clark ME, et al. Delayed rod-mediated dark adaptation is a functional biomarker for incident early age-related macular degeneration. *Ophthalmology*. 2016;123:344–351.
129. Jackson GR, Scott IU, Kim IK, Quillen DA, Iannaccone A, Edwards JG. Diagnostic sensitivity and specificity of dark adaptometry for detection of age-related macular degeneration. *Invest Ophthalmol Vis Sci*. 2014;55:1427–1431.
130. Jeffrey BG, Flynn OJ, Huryn LA, Pfau M, Cukras CA. Scotopic contour deformation detection reveals early rod dysfunction in age-related macular degeneration with and without reticular pseudodrusen. *Invest Ophthalmol Vis Sci*. 2022;63:23.
131. Kim KL, Joo K, Park SJ, Park KH, Woo SJ. Progression from intermediate to neovascular age-related macular degeneration according to drusen subtypes: Bundang AMD cohort study report 3. *Acta Ophthalmol (Copenh)*. 2022;100:e710–e718.
132. Kong M, Kim S, Ham D-I. Incidence of late age-related macular degeneration in eyes with reticular pseudodrusen. *Retina Phila Pa*. 2019;39:1945–1952.
133. Gil JQ, Marques JP, Hoff R, et al. Clinical features and long-term progression of reticular pseudodrusen in age-related macular degeneration: findings from a multicenter cohort. *Eye Lond Engl*. 2017;31:364–371.
134. Sawa M, Ueno C, Gomi F, Nishida K. Incidence and characteristics of neovascularization in fellow eyes of Japanese patients with unilateral retinal angiomatous proliferation. *Retina Phila Pa*. 2014;34:761–767.
135. Pumariega NM, Smith RT, Sohrab MA, LeTien V, Souied EH. A prospective study of reticular macular disease. *Ophthalmology*. 2011;118:1619–1625.
136. Zweifel SA, Imamura Y, Spaide TC, Fujiwara T, Spaide RF. Prevalence and significance of subretinal drusenoid deposits (reticular pseudodrusen) in age-related macular degeneration. *Ophthalmology*. 2010;117:1775–1781.
137. Smith RT, Chan JK, Busuoic M, Sivagnanavel V, Bird AC, Chong NV. Autofluorescence characteristics of early, atrophic, and high-risk fellow eyes in age-related macular degeneration. *Invest Ophthalmol Vis Sci*. 2006;47:5495–5504.
138. Chang YS, Kim JH, Yoo SJ, Lew YJ, Kim J. Fellow-eye neovascularization in unilateral retinal angiomatous proliferation in a Korean population. *Acta Ophthalmol (Copenh)*. 2016;94:e49–53.
139. Joachim N, Mitchell P, Rochtchina E, Tan AG, Wang JJ. Incidence and progression of reticular drusen in age-related macular degeneration: findings from an older Australian cohort. *Ophthalmology*. 2014;121:917–925.
140. Cohen SY, Dubois L, Tadayoni R, Delahaye-Mazza C, Debibie C, Quentel G. Prevalence of reticular pseudodrusen in age-related macular degeneration with newly

Investigative Ophthalmology & Visual Science

diagnosed choroidal neovascularisation. *Br J Ophthalmol*. 2007;91:354–359.

141. Klein R, Meuer SM, Knudtson MD, Iyengar SK, Klein BEK. The epidemiology of retinal reticular drusen. *Am J Ophthalmol*. 2008;145:317–326.
142. Lee MY, Yoon J, Ham D-I. Clinical characteristics of reticular pseudodrusen in Korean patients. *Am J Ophthalmol*. 2012;153:530–535.
143. Arnold JJ, Sarks SH, Killingsworth MC, Sarks JP. Reticular pseudodrusen. A risk factor in age-related maculopathy. *Retina Phila Pa*. 1995;15:183–191.
144. Cleland SC, Domalpally Am Liu Z, et al. Reticular pseudodrusen characteristics and associations in the carotenoids in age-related eye disease study 2 (CAREDS2), an ancillary study of the Women's Health Initiative. *Ophthalmol Retina*. 2021;5:721–729.
145. Zouache MA, Bennion A, Hageman JL, Pappas C, Richards BT, Hageman GS. Macular retinal thickness differs markedly in age-related macular degeneration driven by risk polymorphisms on chromosomes 1 and 10. *Sci Rep*. 2020;10:21093.
146. Thee EF, Colijn JM, Cougnard-Grégoire A, et al. The phenotypic course of age-related macular degeneration for ARMS2/HTRA1: The EYE-RISK Consortium. *Ophthalmology*. 2022;129(7):752–764.
147. Schmitz-Valckenberg S, Fleckenstein M, Zouache MA, et al. Progression of age-related macular degeneration among individuals homozygous for risk alleles on Chromosome 1 (CFH-CFHR5) or Chromosome 10 (ARMS2/HTRA1) or both. *JAMA Ophthalmol*. 2022;140:252–260.
148. Kaye RA, Patasova K, Patel PJ, Hysi P, Lotery AJ. Macular thickness varies with age-related macular degeneration genetic risk variants in the UK Biobank cohort. *Sci Rep*. 2021;11:23255.
149. Pinilla I, Garcia-Martin E, Fernandez-Larripa S, Fuentes-Broto L, Sanchez-Cano AI, Abecia E. Reproducibility and repeatability of Cirrus and Spectralis Fourier-domain optical coherence tomography of healthy and epiretinal membrane eyes. *Retina Phila Pa*. 2013;33:1448–1455.
150. Suzuki M, Sato T, Spaide RF. Pseudodrusen subtypes as delineated by multimodal imaging of the fundus. *Am J Ophthalmol*. 2014;157:1005–1012.
151. Chan H, Cougnard-Grégoire A, Delyfer MN, et al. Multimodal imaging of reticular pseudodrusen in a population-based setting: The Alienor Study. *Invest Ophthalmol Vis Sci*. 2016;57:3058–3065.
152. Smith RT, Sohrab MA, Busuioc M, Barile G. Reticular macular disease. *Am J Ophthalmol*. 2009;148:733–743.e2.
153. Cohen SY, Dubois L, Tadayoni R, Delahaye-Mazza C, Debibie C, Quentel G. Prevalence of reticular pseudodrusen in age-related macular degeneration with newly diagnosed choroidal neovascularisation. *Br J Ophthalmol*. 2007;91:354–359.
154. Ueda-Arakawa N, Ooto S, Tsujikawa A, Yamashiro K, Oishi A, Yoshimura N. Sensitivity and specificity of detecting reticular pseudodrusen in multimodal imaging in Japanese patients. *Retina*. 2013;33:490–497.